Time-Domain Vector-Potential Analysis of Transmission-Line Problems

Natalia Georgieva, *Student Member, IEEE*, and Eikichi Yamashita, *Fellow, IEEE*

***Abstract*— A time-domain vector-potential (TDVP) approach for the analysis of transient electromagnetic fields is proposed in this paper. The field is analyzed by the magnetic VP for which the wave equation is solved by a finite-difference (FD) scheme. The feasibility of the method has been shown by simulations of several transmission-line problems. The results have been compared with reported data obtained by the conventional finite-difference time-domain (FDTD) method, empirical formulas, and measurements. The proposed approach is not inferior to the FDTD method in terms of generality and memory requirements. At the same time, a reduction of central processing unit (CPU) time is achieved because only three scalar wave equations are solved instead of the six Maxwell equations for all field components. It has also been shown that there are certain structures where the components of the magnetic VP are decoupled, which implies the possibility for a consecutive algorithm with reduced memory requirements.**

***Index Terms*— Electromagnetic transient propagation, FDTD method, time-domain analysis.**

I. Introduction

THE construction of solutions in terms of vector potentials (VP's) is a well-known approach in electromagnetics. An important advantage of the field VP's is that they are smoother functions of space than the field vectors in the vicinity of sources and sharp discontinuities such as edges, wedges, and corners. Besides that, the electromagnetic field can be described by a reduced number of scalar functions where the choice of the VP depends on the boundary conditions and excitation [1].

VP approaches are often applied in frequency-domain analysis. However, in time-domain methods there are only a few examples for the application of the VP's, which can be found exclusively in the algorithms based on the time-domain surface integral equations [2]–[4]. There the VP's are viewed as the free-space contribution of equivalent surface currents and are computed mostly via integration. The possibility for a finite-difference time–space analysis based on the wave equation of the magnetic VP $\vec{A}$ was first observed in [5], where it is noted that although the approach has never been implemented it would prove not only faster, but also advantageous (in respect to memory requirements) since the solutions for the three components of $\vec{A}$ are decoupled into three scalar wave equations after the Lorentz's gauge condition is imposed. Thus, the overall computation could be separated into three consecutive parts with less memory load, but with the same computation time. As will be shown below, the decoupling of the $\vec{A}$ components is not generally true, e.g., in the case of a sharp change of the dielectric constant (dielectric interface) or in the vicinity of edges and wedges.

The possibility for a reduction of the computation time by the solution of three wave equations instead of the Maxwell's curl equations was observed and applied in some modifications of the conventional finite-difference time-domain (FDTD) algorithm [6], [7]. Both [6] and [7] show a successful analysis of the field propagation only in terms of the electric field $\vec{E}$ for which the wave equation is solved. In [6], the algorithm is based on a direct solution of the vector wave equation where all three components of $\vec{E}$ are coupled through the $\nabla \times \nabla \times$ operator. In [7], the vector wave equation is further reduced to three independent scalar wave equations for all homogeneous subregions where the condition $\nabla \cdot \vec{E} = 0$ holds. The solution is coupled with the vector wave equation at nondivergence-free regions. In [6] and [7], a reduction of central processing unit (CPU) time of approximately 30%–35% was reported. Computer-memory requirements of the algorithm presented in [7] were reduced by approximately 1/3 in the case of planar structures.

In this paper, we propose a finite-difference (FD) time–space approach which is based on the calculation of $\vec{A}$ by the scalar wave equations. It has all advantages of the wave-equation analyses briefly reviewed above—reduced CPU time and a possibility for memory reduction when decoupling of the components of $\vec{A}$ is present. In addition, its versatility is the same as that of the conventional FDTD method. There are cases where the field could actually be represented by only two or even one component of $\vec{A}$, e.g., scattering from infinitesimally thin perfectly conducting plates, wire antennas, etc. Its implementation is simple and can be generalized to complex geometries. As with all FD schemes, it suffers from two basic shortcomings—it needs an absorbing boundary condition (ABC) whenever outward propagation is to be simulated, and it has a numerical dispersion similar to the Yee algorithm for a given ratio of the discretization steps in space and time. On the other hand, the smoother behavior of the VP in the vicinity of sharp discontinuities implies less numerical errors for a given space discretization.

II. Basic Equations

A. VP Formulation

Potential functions are typically introduced to represent the fields created by induced currents and charges which are related to the currents via the continuity relation. From

Manuscript received April 27, 1997; revised January 14, 1998.

N. Georgieva was with the Department of Electronic Engineering, University of Electro-Communications, Chofu-shi, Tokyo 182, Japan. She is now with Dalhousie University Polytechnic, Halifax, N.S., Canada B3J 1B6.

E. Yamashita is with the Department of Electronic Engineering, University of Electro-Communications, Chofu-shi, Tokyo 182, Japan.

Publisher Item Identifier S 0018-9480(98)02731-8.

Maxwell equations, it follows that the field vectors $\vec{E}$ and $\vec{H}$ are related to the magnetic VP $\vec{\mathcal{A}}$ and the electric scalar potential φ as

$$\vec{E} = -\frac{\partial \vec{\mathcal{A}}}{\partial t} - \nabla\varphi \tag{1}$$

$$\vec{H} = \frac{1}{\mu}\nabla \times \vec{\mathcal{A}}. \tag{2}$$

The VP $\vec{\mathcal{A}}$ satisfies the wave equation

$$\Delta\vec{\mathcal{A}} - \mu\epsilon\frac{\partial^2 \vec{\mathcal{A}}}{\partial t^2} = -\mu\vec{J} \tag{3}$$

if the scalar potential is related to $\vec{\mathcal{A}}$ by the Lorentz's gauge condition

$$\mu\epsilon\frac{\partial\varphi}{\partial t} = -\nabla\cdot\vec{\mathcal{A}}. \tag{4}$$

From (4), it follows that the field vectors can be conveniently expressed only by the magnetic VP $\vec{\mathcal{A}}$ as

$$\frac{\partial \vec{E}}{\partial t} = -\frac{\partial^2 \vec{\mathcal{A}}}{\partial t^2} + \frac{1}{\mu\epsilon}\nabla\nabla\cdot\vec{\mathcal{A}} \tag{5}$$

$$\vec{H} = \frac{1}{\mu_0}\nabla\times\vec{\mathcal{A}}. \tag{6}$$

From (3), it is obvious that the three VP components' solutions are decoupled for all internal points of every homogeneous subregion. It can be solved for each component of $\vec{\mathcal{A}}$ using standard FD techniques. As will be shown below, coupling appears at conducting surfaces of finite extent and also at dielectric interfaces.

B. Boundary Conditions and Coupling of the VP Components at Interfaces

Only planar boundaries and interfaces will be considered here because the derivation of the relations for the Cartesian components of $\vec{\mathcal{A}}$ is straightforward. It is also assumed that there are no magnetic materials present in the structure. The unit normal $\hat{n}$ is assumed to point from regions 1 to 2. The normal component of $\vec{\mathcal{A}}$ will be denoted by $\mathcal{A}_n$. The tangential component of $\vec{\mathcal{A}}$ will be denoted by

$$\vec{\mathcal{A}}_\tau = \mathcal{A}_{\xi_1}\hat{\xi}_1 + \mathcal{A}_{\xi_2}\hat{\xi}_2$$

where $(\hat{\xi}_1, \hat{\xi}_2)$ are the unit tangents of the planar surface.

1) Dielectric Interfaces: The continuity of the tangential $\vec{H}$ components leads to the following relations for the normal and tangential components of $\vec{\mathcal{A}}$ at the interface

$$\mathcal{A}_n^{(10} = \mathcal{A}_n^{(2)} \tag{7}$$

$$\vec{\mathcal{A}}_\tau^{(1)} = \vec{\mathcal{A}}_\tau^{(2)}$$

$$\frac{\partial \vec{\mathcal{A}}_\tau^{(1)}}{\partial n} = \frac{\partial \vec{\mathcal{A}}_\tau^{(2)}}{\partial n}. \tag{8}$$

While (8) is enough to uniquely define the tangential $\vec{\mathcal{A}}_\tau$ components, the normal $\mathcal{A}_n$ component cannot be calculated by the single relation (7). Here, an additional continuity relation will be used—the continuity of the scalar potential φ which follows from the continuity of the tangential $\vec{E}$ components and the first of (8)

$$\frac{1}{\mu_0\epsilon_1}\left(\frac{\partial \mathcal{A}_n^{(1)}}{\partial n} + \frac{\partial \mathcal{A}_{\xi_1}^{(1)}}{\partial \xi_1} + \frac{\partial \mathcal{A}_{\xi_2}^{(1)}}{\partial \xi_2}\right) = \frac{1}{\mu_0\epsilon_2}\left(\frac{\partial \mathcal{A}_n^{(2)}}{\partial n} + \frac{\partial \mathcal{A}_{\xi_1}^{(2)}}{\partial \xi_1} + \frac{\partial \mathcal{A}_{\xi_2}^{(2)}}{\partial \xi_2}\right). \tag{9}$$

Bearing in mind that

$$\mathcal{A}_{\xi_i}^{(1)} = \mathcal{A}_{\xi_i}^{(2)}, \qquad i = 1, 2$$

one more relation for the $\mathcal{A}_n$ component is obtained as follows:

$$\epsilon_2\frac{\partial \mathcal{A}_n^{(1)}}{\partial n} - \epsilon_1\frac{\partial \mathcal{A}_n^{(2)}}{\partial n} = (\epsilon_1 - \epsilon_2)\left(\frac{\partial \mathcal{A}_{\xi_1}}{\partial \xi_1} + \frac{\partial \mathcal{A}_{xi_2}}{\partial \xi_2}\right). \tag{10}$$

Equations (7) and (10) completely define the value of $\mathcal{A}_n$ at the interface. It is worth noting that the presence of a dielectric-to-dielectric interface couples the normal component of $\vec{\mathcal{A}}$ with its tangential components. First, the tangential components at the interface are updated independently using their most recent values at the internal points of the neighboring regions. Then, the computation of the most recent values of the normal component at the interface takes place. Obviously, the components are decoupled if $\epsilon_1 = \epsilon_2$, and in this case, each component simply satisfies its wave equation.

2) Electric Wall: This is a boundary at which the condition

$$\varphi(x, y, z, t) = \text{const} \tag{11}$$

can be imposed. Typical examples are the infinite ground plane of a microstrip-line structure (see Fig. 2) or the walls of a waveguide. Since

$$\hat{n}\times\vec{E} = 0 \tag{12}$$

(11) implies that the boundary conditions for the components of $\vec{A}$ are

$$\frac{\partial \mathcal{A}_n}{\partial n} = 0 \tag{13}$$

$$\vec{\mathcal{A}}_\tau = 0. \tag{14}$$

3) Magnetic Wall: This boundary condition is used when the structure (including the excitation) is symmetrical in respect to a given plane. It is equivalent to setting the tangential components of the $\vec{H}$ field equal to zero. Therefore, the boundary conditions for $\vec{\mathcal{A}}$ in this case are defined as

$$\mathcal{A}_n = 0 \tag{15}$$

$$\frac{\partial \mathcal{A}_{\xi_i}}{\partial n} = 0, \qquad i = 1, 2. \tag{16}$$

4) Infinitesimally Thin Finite-Size Conducting Patches at Interfaces: In this case, (12) holds, as it holds also for the ground plane. However, unlike the ground plane, the scalar potential cannot be set equal to a constant. Hereafter, such conducting surfaces will be referred to as *floating conductors*. At floating conductors of infinitesimally small thickness, the value of the scalar potential is the same for both regions as follows:

$$\varphi^{(1)} = \varphi^{(2)}. \tag{17}$$

The above relation is identical with (9) or (10). As follows from (12) and (17), the tangential components of $\vec{\mathcal{A}}$ should

also be continuous functions ($\mathcal{A}_{\xi_i}^{(1)} = \mathcal{A}_{\xi_i}^{(2)}, i = 1, 2$), and can be calculated explicitly as

$$\frac{\partial \mathcal{A}_{\xi_i}}{\partial t} = -\frac{\partial \varphi}{\partial \xi_i}, \qquad i = 1, 2. \tag{18}$$

Substituting the Lorentz's gauge condition in (18) leads to the relation

$$\frac{\partial^2 \mathcal{A}_{\xi_i}}{\partial t^2} = \frac{1}{\mu_0 \epsilon_1} \frac{\partial}{\partial \xi_i} \left(\frac{\partial \mathcal{A}_n^{(1)}}{\partial n} + \frac{\partial \mathcal{A}_{\xi_1}}{\partial \xi_1} + \frac{\partial \mathcal{A}_{\xi_2}}{\partial \xi_2} \right). \tag{19}$$

The continuity of the scalar potential implies that the same value for $\mathcal{A}_{\xi_i}$ would be obtained if the equation

$$\frac{\partial^2 \mathcal{A}_{\xi_i}}{\partial t^2} = \frac{1}{\mu_o \epsilon_2} \frac{\partial}{\partial \xi_i} \left(\frac{\partial \mathcal{A}_n^{(2)}}{\partial n} + \frac{\partial \mathcal{A}_{\xi_1}}{\partial \xi_1} + \frac{\partial \mathcal{A}_{\xi_2}}{\partial \xi_2} \right), \qquad i = 1, 2$$

is used. Once the tangential $\vec{\mathcal{A}}$ components are updated, the values of the $\mathcal{A}_n$ component at the conducting patch are computed using relations identical to (7) and (10).

It must be noted that although the procedure for the calculation of the $\mathcal{A}_n$ component at dielectric-to-dielectric interfaces and at infinitesimally thin floating conductors is the same as it follows from the continuity of the scalar potential, the procedure for the tangential components is entirely different, as is seen from (8) and (19). While at dielectric-to-dielectric interfaces, the $\vec{\mathcal{A}}_\tau$ components are self-dependent, at conducting interface patches they depend on the normal derivative of $\mathcal{A}_n$. The points at such patches become points of generation of $\vec{\mathcal{A}}_\tau$ under the influence of $\mathcal{A}_n$. When the interface patch is immersed in a homogeneous region ($\epsilon_1 = \epsilon_2$), $\mathcal{A}_n$ no longer depends on $\vec{\mathcal{A}}_\tau$ [see (10)], but it still generates the values of the tangential components through (19).

5) Conducting Bodies of Finite Size: The application of the boundary condition (12) at the surface of a conducting body of a finite size is less complicated than the previous case. It includes the condition

$$\frac{\mathcal{A}_n}{\partial n} = 0 \tag{20}$$

at all surface points not coinciding with wedges and corners. Since the tangential components are again obtained by (19), it can be shown that coupling among the $\vec{\mathcal{A}}$ components appears exactly at the edge points of the surface. This phenomenon is best described when the $\mathcal{A}_{\xi_i}$ component is displaced from the $(\mathcal{A}_{\xi_j}, \mathcal{A}_{\xi_k})$ components by a half-space step along the ξ_i coordinate. Here, $(\xi_{i,j,k}, i, j, k = 1, 2, 3, i \neq j \neq k)$ denote the respective components of $\vec{\mathcal{A}}$ (see Fig. 1). In the case of infinitesimally thin conducting patches, it is numerically more convenient to adjust the meshes of the normal and tangential components so that they coincide along the axis normal to the patch.

III. Numerical Implementation

A. Discretization of the Space-Time Domain

For the analysis of the planar structure in Fig. 2, the meshes of $\mathcal{A}_x$, $\mathcal{A}_y$, $\mathcal{A}_z$ coincide along the x-axis. At every $x = \text{const}$ plane, the components are displaced by half a step, as described at the end of the previous section and in Fig. 1. This displacement gives the most exact numerical treatment of the surface operators $\nabla_s \nabla_s \cdot$ and $\nabla_s \cdot$ by a central-difference scheme. These operators are encountered in the boundary-condition relations (10) and (19).

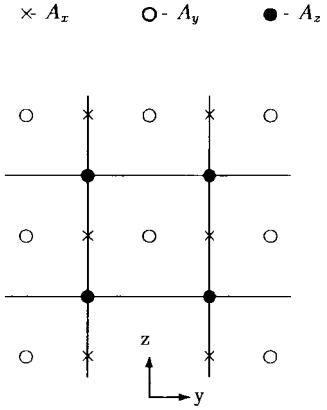

Fig. 1. Space displacement of $\vec{\mathcal{A}}$ components at a $x = \text{const}$ plane.

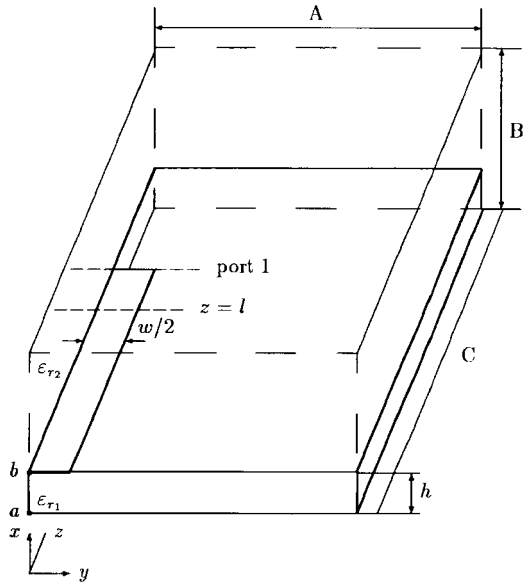

Fig. 2. Computational domain for the microstrip open end.

All three components of $\vec{\mathcal{A}}$ are calculated at the same moments of time $t = k\Delta t$. This also refers to the $\vec{H}$ field. The electric field $\vec{E}$ is calculated at $t = (k + 1/2)\Delta t$, as follows from (5). The field vectors are not needed in the basic algorithm. They are calculated for the purpose of post-processing computations of the structure's parameters only when and where it is necessary.

The time-step Δt and the space-step Δh are related to the higher speed of light in the structure $\boldsymbol{c}$ by

$$\Delta t = \frac{\Delta h}{cq} \tag{21}$$

where q should satisfy the Courant stability condition

$$q \geq \sqrt{3}.$$

In the presented simulations, q was set to $q = 2$. The space-step has to be chosen small enough in order to obtain accurate field behavior at discontinuities and at higher frequencies. Usually the following recommendation is followed [8], [11]:

$$\Delta h \leq \frac{\lambda_{\min}}{8} \tag{22}$$

where $\lambda_{\min}$ is the shortest wavelength of interest.

B. Defining the Excitation Pulse

The excitation pulse in the case of transmission-line problems is usually chosen to be a Gaussian pulse in time as follows:

$$g(t) = \exp[-\alpha(t - t_0)^2] \tag{23}$$

where t_0 is the temporal moment at which the pulse is located. The Fourier transform of this pulse is a Gaussian function of frequency

$$G(f) \approx \exp\left[-\frac{\pi^2 f^2}{\alpha}\right]. \tag{24}$$

If frequency data are needed up to a maximum frequency of $f_{\max}$, then the pulse must have wide enough spectrum to cover the $(0 \div f_{\max})$ band. The value of α must be chosen properly. On the other hand, α must be a function of the number of time-steps β from truncation to maximum of the time-domain Gaussian pulse to ensure smooth enough launch of the pulse [5]

$$\alpha = \left(\frac{\eta}{\beta \Delta t}\right)^2. \tag{25}$$

If, for example, a truncation level of approximately -140 dB is desired, then η has to be set to $\eta = 4$. We shall also require that the spectrum of the Gaussian pulse at $f_{\max}$ has at least a value of $G(f_{\max}) = 0.1$. The relation between β and $f_{\max}$ is readily obtained as

$$\beta = \frac{\eta\sqrt{\ln 10}}{\pi f_{\max} \Delta t}. \tag{26}$$

The temporal step is firmly determined by (21). Therefore, the above equation can be written in terms of $\lambda_{\min}$ and Δh as

$$\beta = \frac{\eta g \sqrt{\ln 10}\sqrt{\mu_r \epsilon_r}}{\pi}\left(\frac{\lambda_{\min}}{\Delta h}\right) \tag{27}$$

where the ratio $\lambda_{\min}/\Delta h$ is set by (22). Equation (27) defines the appropriate width of the Gaussian pulse in time.

C. The FD Wave Equation and Boundary Relations

Each component $\xi = x, y, z$ of the auxiliary vector $\vec{A} = \vec{\mathcal{A}}/(\mu_0 \Delta h)$ is calculated by an explicit FD scheme of the wave equation [8]

$$D_{tt}^2\{\mathcal{A}_\xi\} = \alpha^2(L\{\mathcal{A}_\xi\} + J_{s_\xi}) \tag{28}$$

where: 1) $\alpha = 1/(q\sqrt{\epsilon_{r_i}\mu_{r_i}}), i$ is the region index; 2) $L = D_{xx}^2 + D_{yy}^2 + D_{zz}^2$ is the FD Laplace operator; and 3) J_{s_ξ} is the excitation surface current (if present).

The excitation is in the form of surface currents because of the normalization of $\vec{\mathcal{A}}$ in respect to the space step Δh. The time derivative of A_ξ is first calculated as

$$D_t^{k+1/2}\{A_\xi\} = D_t^{k-1/2}\{A_\xi\} + \alpha^2(L\{A_\xi^k\} + J_{s_\xi}^k).$$

The value of A_ξ is then calculated as

$$A_\xi^{k+1} = A_\xi^k + D_t^{k+1/2}\{A_\xi\}.$$

The boundary values of the VP components are calculated by the discretized form of the boundary relations given in Section II-2. Here, the explicit discretized form of the boundary relations at the dielectric interface only will be given (8), (7), (10). Equations (13), (14)–(16), and (19) are implemented in a similar manner.

The discretized form of (8) for the interface values of the tangential components of $\vec{A}$ is

$$A_{\xi_o} = \frac{4(A_{\xi_{-1}}^{(1)} + A_{\xi_{+1}}^{(2)} - (A_{\xi_{-2}}^{(1)} + A_{\xi_{+2}}^{(2)})}{6}. \tag{29}$$

Here, the superscripts denote the respective region, and the subscripts give the position along the normal of the interface which points from region 1 to region 2. In the derivation of this formula, the second-order backward/forward approximation of the normal derivative has been used as follows:

$$\frac{\partial f_i^{\mp}}{\partial x} = \frac{\pm 3 f_i \mp 4 f_{i\mp 1} \pm f_{i\mp 2}}{2\Delta h}. \tag{30}$$

Equations (7) and (10) lead to the following expression:

$$A_{n_o} = \frac{1}{3(\epsilon_1 + \epsilon_2)}[4(\epsilon_2 A_{n_{-1}}^{(1)} + \epsilon_1 A_{n_{+1}}^{(2)}) - (\epsilon_2 A_{n_{-2}}^{(1)} + \epsilon_1 A_{n_{+2}}^{(2)}) + 2(\epsilon_1 - \epsilon_2)(D_{\xi_1}\{A_{\xi_1}\} + D_{\xi_2}\{A_{\xi_2}\})]. \tag{31}$$

Here, the operator $D_{\xi_i}\ i = 1, 2$ represents finite differences along the coordinate ξ_i.

Once $\vec{A}$ is calculated, the field vectors can be obtained by the discretized form of (5) and (6) and used in the computation of certain parameters of the structure.

D. The Transmitting Boundary for the Wave Equation

The ABC's pose a serious problem for time-domain FD schemes, and is still intensively studied. There are many numerical approximations of the ABC, but they are either with high memory and CPU time requirements, or their performance is very much dependent on the angle of incidence and dispersion of the propagating pulse. Here, it was chosen to apply the first-order Liao extrapolation scheme [9], [10]. The boundary value is thus obtained by a second-order Lagrange interpolation of the field values inside the region at a point where location depends on the dielectric constant of the region and the parameter q, which was defined in (21).

IV. Results and Discussion

The results of the simulations of different microstrip-line discontinuities are presented—an open end, a gap, and a double change in the width of the line. The discontinuities are described by the dispersion of their S-parameters. The dispersion characteristics of the homogeneous microstrip line were also calculated using the incident-field transient data.

The geometry of the numerical region is shown in Fig. 2. The excitation plane is at $z = 0$. The excitation is in the form of J_x electric currents, which are a Gaussian function of time. While the pulse is launched, a symmetry condition for A_x and A_y, and an antisymmetry condition for A_z, are imposed (magnetic wall). At a later moment, the radiation condition is switched on so that reflections could be absorbed. This moment is carefully chosen after the pulse is entirely launched and before reflections could reach the back plane.

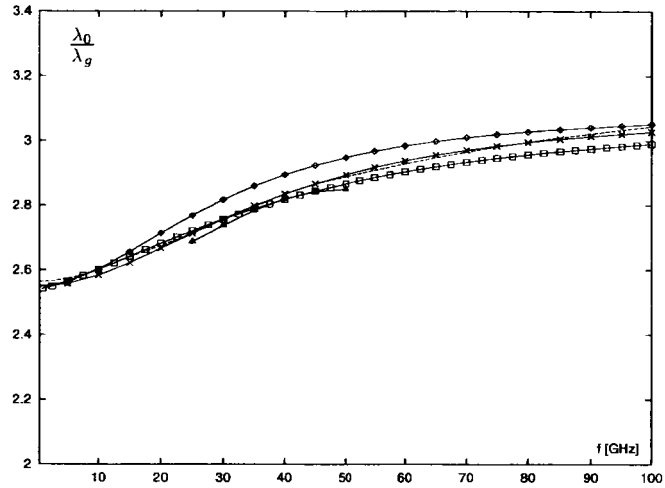

Fig. 3. Relative guide wavelength λ_0/λ_g of a microstrip line: $w = 0.6$ mm, $h = 0.6$ mm, $\epsilon_{r_1} = 9.6$ mm. With boxes: empirical formula of Hammerstad and Jensen [17], with crosses: empirical formula of Pramanick and Bhartia [14], with triangles: results of Katehi and Alexopoulos [13], with diamonds: empirical formula of Edwards and Owens, dashed line: current approach.

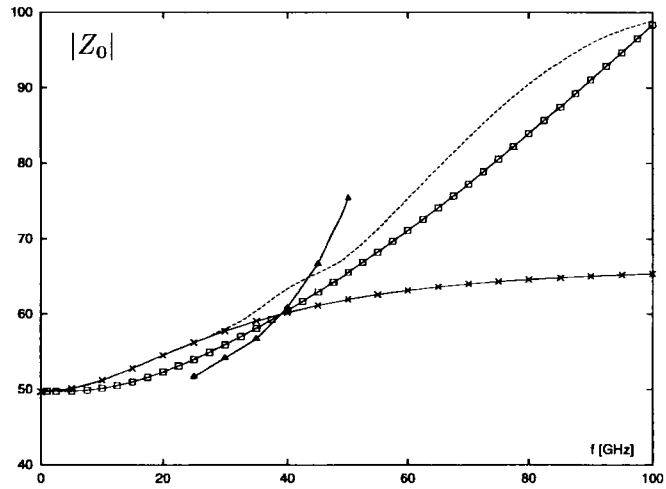

Fig. 4. Relative guide wavelength λ_0/λ_g of a microstrip line: $w = 0.6$ mm, $h = 0.6$ mm, $\epsilon_{r_1} = 9.6$ mm. With boxes: empirical formula of Kobayashi [16], with crosses: empirical formula of Edwards and Owens [15], with triangles: results of Katehi and Alexopoulos [13], dashed line: current approach.

Since all analyzed structures are symmetrical in respect to the $y = 0$ plane, a magnetic-wall boundary conditions are imposed for $\vec{A}$ at this plane.

The dimensions of the numerical region are: 1) width $A = 4w$; 2) height $B = 4h$; and 3) length $C = 180\Delta h$. Here, Δh denotes the space discretization step, w is the strip width, and h is the substrate thickness.

A. Dispersion Characteristics of a Microstrip Line

The analyzed microstrip line has the following dimensions: $w = 0.6$ mm, $h = 0.6$ mm, and strip thickness t is assumed equal to zero. The dielectric constant of the substrate is $\epsilon_{r_1} = 9.6$. This structure was chosen for the purpose of comparison with data reported in [11]–[13]. The dispersion characteristics of the line were obtained from the transient response of the incident strip current and voltage at two reference points along the line [11]. The relative guide propagation constant

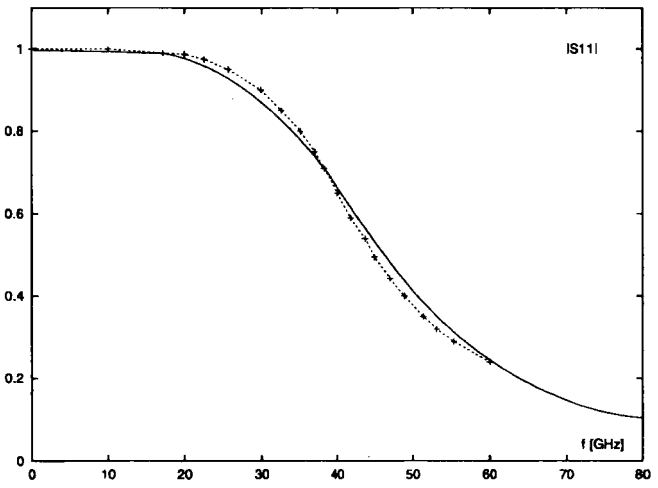

Fig. 5. $|S_{11}|$ for the open end. With crosses: as in [12], with line: current approach.

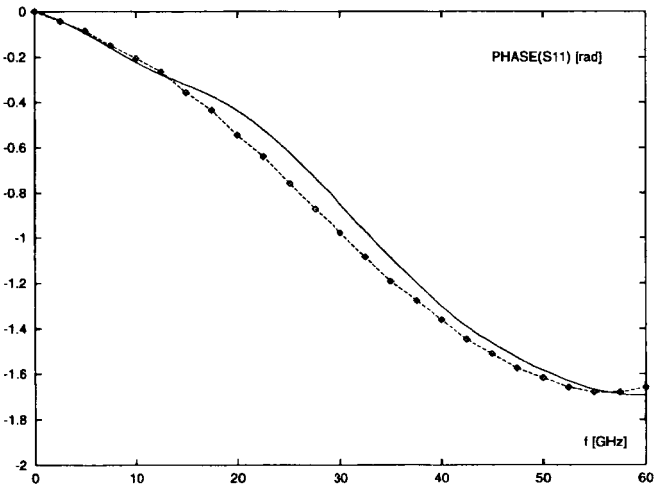

Fig. 6. Phase of $|S_{11}|$ for the open end. With boxes: as in [12], with line: current approach.

$\lambda_0/\lambda_g = \sqrt{\epsilon_{r_{\text{eff}}}}$ has been calculated as a function of frequency and the results have been compared with those given in [13] (frequency-domain calculations), with the empirical formulas of Pramanick and Bhartia [14], Edwards and Owens [15], and Kobayashi [16] (see Fig. 3). The results of the present method are in very good agreement with the already existing data.

The calculations for the characteristic impedance $|Z_0|$ are presented in Fig. 4 and compared with those provided in [13], with the empirical formulas of Edwards and Owens [15] and Hammerstad and Jensen [17]. Unlike the results for the propagation constant, there is quite a discrepancy in the $|Z_0|$ data obtained by the different methods. The results of the time-domain vector-potential (TDVP) approach are closest to the calculations with the formula of Hammerstad and Jensen, which is considered to be one of the best approximations in the computer-aided design (CAD) of microstrips.

B. Open-End Microstrip Line

The open-end discontinuity was also analyzed by the TDVP approach for various microstrip lines. Here, the results for the same microstrip line will be presented: $w = 0.6$ mm, $h = 0.6$

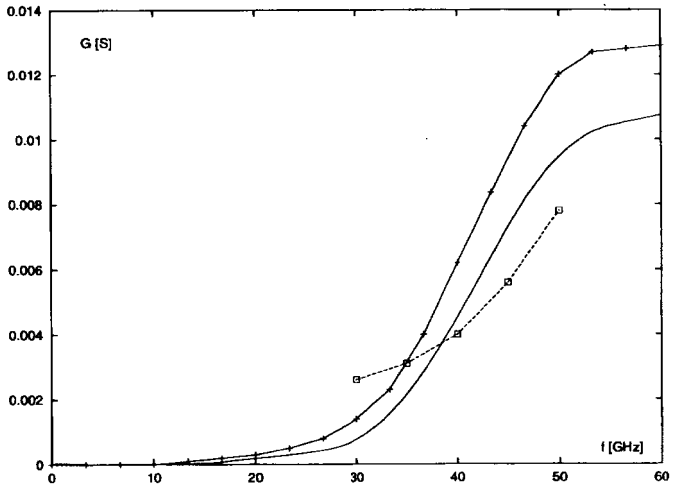

Fig. 7. Radiation conductance $G_{(f)}$ of the open-end line. With crosses: as in [12], with boxes: as in [13], with line: current approach.

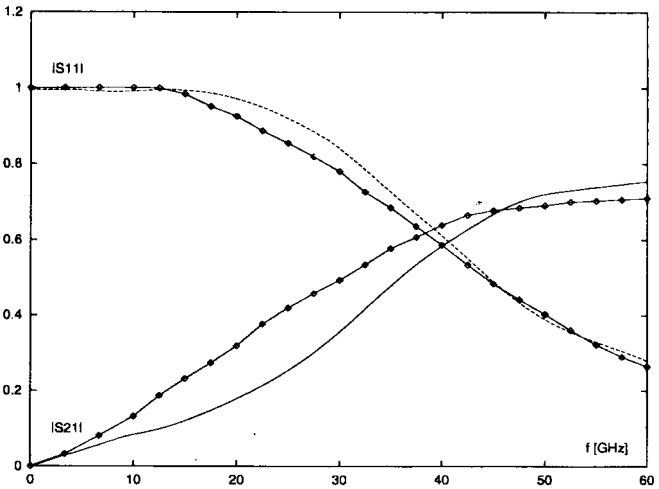

Fig. 9. $|S_{11}|$ and $|S_{21}|$ for the gap discontinuity. With boxes: as in [12], with lines: current approach.

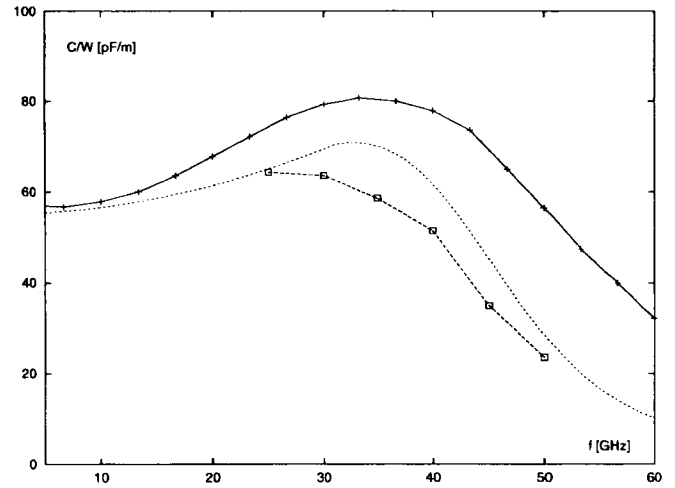

Fig. 8. Normalized capacitance $C_{(f)}/w$ of the open-end line. With crosses: as in [12], with boxes: as in [13], with line: current approach.

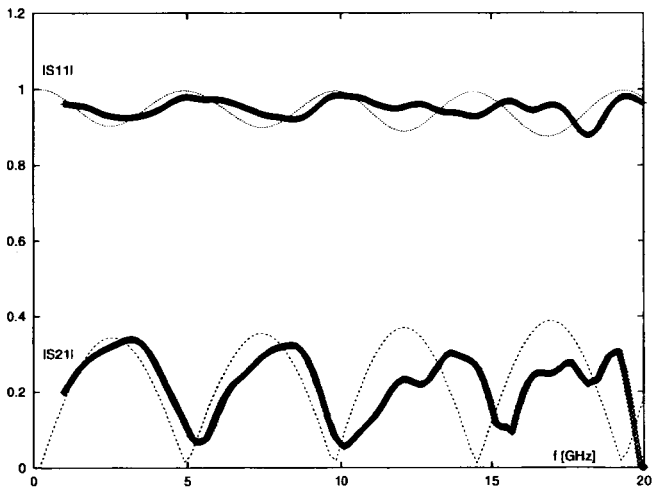

Fig. 10. $|S_{11}|$ and $|S_{21}|$ for the double step-in-width, discontinuity, $\epsilon_{r_1} = 10.2$. With thick lines: measurements, with lines: current approach.

mm, $\epsilon_{r_1} = 9.6$. The magnitude of S_{11} is plotted in Fig. 5 and is compared with the results given in [12]. The same comparison is made for the phase of S_{11} in Fig. 6. The results obtained by the present method are in good agreement with those obtained by the Yee FDTD algorithm for the magnitude of S_{11}, but there are differences in the calculations of the phase dispersion of S_{11}. That is why the complex S_{11} was used to calculate the equivalent conductance (representing radiation losses) and the equivalent normalized capacitance C/w for which data are available in [12] and [13]. These results are given in Figs. 7 and 8, respectively. The $G(f)$ curve obtained by the TDVP algorithm has the same character as the one given in [12], but it is shifted toward higher frequencies, i.e., toward the values obtained by Katehi and Alexopoulos [13]. A shift toward the frequency-domain results of [13] at higher frequencies is also observed in the $C(f)/w$ curve. Obviously, the equivalent parameters' dispersion is very sensitive to even slight changes in the results for the complex reflection coefficient.

C. Gap Discontinuity

This discontinuity was also simulated for the microstrip line from the previous cases. The gap width is chosen $s = 0.5h$, exactly as in [12]. The results for the magnitudes of S_{11} and S_{21} are shown in Fig. 9. While there is good agreement in the results for $|S_{11}|$, $|S_{21}|$ results show substantial difference especially at lower frequencies. However, it must be noted that the almost linear behavior of the $|S_{21}|(f)$ curve provided in [12] is in some contradiction with the highly nonlinear curve of $|S_{11}|(f)$ at lower frequencies.

D. Double Step-in-Width Discontinuity

The discontinuity is simulated for a transmission line of dimensions $w = 0.56$ mm and $h = 0.64$ mm. The dielectric constant of the substrate is $\epsilon_{r_1} = 10.2$. The strip width changes from w to $w_d = 2\ w$ and back to w. The length of the strip with a width of w_d is $l_d = 10$ mm. This structure has resonant properties and its investigation was important in order to verify the validity of the approach when lengthy calculations with multiple reflected signals take place. It is well known that the accumulated numerical errors in time-stepping procedures badly affect the late-time transient results. The reflection and transmission coefficient of a real test line with the above

parameters were measured in order to provide some basis for comparison with the simulated data. The experimental and simulation results are presented in Fig. 10.

V. Conclusion

A TDVP technique for the analysis of transient fields is proposed in this paper and applied to transmission-line problems. This numerical approach has the advantage of decreased CPU time approximately 30% in comparison with the FDTD method. A possibility for memory savings and further reduction of computation time exists in applications to specific problems like scattering and radiation from thin plates and wires in a homogeneous medium. The advantages of the VP time-domain analysis and its applicability to a wide variety of problems is still to be investigated. So far, its feasibility has been proven by the simulation of three types of microstrip-line discontinuities. Further improving of the ABC's and increasing the numerical efficiency could make the algorithm a useful numerical tool for the analysis of complex structures.

Acknowledgment

The authors would like to thank Prof. Kishi and Prof. Ma for their support and advice concerning the theoretical background of the method, and for the helpful discussion of many practical aspects of its application.

References

[1] R. F. Harrington, *Time-Harmonic Electromagnetic Fields*. New York: McGraw-Hill, 1961.
[2] L. B. Felsen, Ed., *Transient Electromagnetic Fields*. Berlin, Germany: Springer-Verlag, 1976.
[3] D. A. Vechinski, S. M. Rao, and T. K. Sarkar, "Transient scattering from three-dimensional arbitrarily shaped dielectric bodies," *J Opt. Soc. Amer. A, Opt. Image Sci.*, vol. 11, no. 4, pp. 1458–1470, Apr. 1994.
[4] N. Georgieva and E. Yamashita, "Finite difference approach to the solution of time-domain integral equations for layered structures," *IEEE Trans. Microwave Theory Tech.*, vol. 45, pp. 984–990, June 1997.
[5] K. S. Kunz and R. J. Luebbers, *Finite-Difference Time-Domain Method for Electromagnetics*. Boca Raton, FL: CRC Press, 1993.
[6] D. Krupezevic, V. Brankovic, and F. Arndt, "The wave-equation FDTD for efficient eigenvalue analysis and S-matrix computation of waveguide structures," *IEEE Trans. Microwave Theory Tech.*, vol. 41, pp. 2109–2115, Dec. 1993.
[7] P. Aoyagi, J.-F. Lee, and R. Mittra, "A hybrid Yee algorithm/scalar-wave equation approach," *IEEE Trans. Microwave Theory Tech.*, vol. 41, pp. 1593–1600, Sept. 1993.
[8] J. C. Strikwerda, *Finite Difference Schemes and Partial Differential Equations* (Mathematics Series). Pacific Grove, CA: Brooks/Cole, 1989.
[9] Z. P. Liao, H. L. Wong, Y. Baipo, and Y. Yifan, "A transmitting boundary for transient wave analyzes," *Scientia*, vol. XXVII, no. 10, pp. 1063–1076, Oct. 1984.
[10] A. Taflove, *The Finite-Difference Time-Domain Method*. Norwood, MA: Artech House, 1995.
[11] X. Zhang, J. Fang, K. Mei, and Y. Liu, "Calculations of the dispersive characteristics of microstrips by the time-domain finite difference method," *IEEE Trans. Microwave Theory Tech.*, vol. 36, pp. 263–267, Feb. 1988.
[12] X. Zhang and K. K. Mei, "Time-domain finite-difference approach to the calculation of the frequency-dependent characteristics of microstrip discontinuities," *IEEE Trans. Microwave Theory Tech.*, vol. 36, pp. 1775–1787, Dec. 1988.
[13] P. B. Katehi and N. G. Alexopoulos, "Frequency-dependent characteristics of microstrip discontinuities in millimeter-wave integrated circuits," *IEEE Trans. Microwave Theory Tech.*, vol. MTT-33, pp. 1029–1035, Oct. 1985.
[14] P. Pramanick and P. Bhartia, "An accurate description of dispersion in microstrip," *Microwave J.*, vol. 26, no. 12, pp. 89–96, Dec. 1983.
[15] K. C. Gupta, R. Garg, and R. Chadha, *Computer-Aided Design of Microwave Circuits*. Norwood, MA: Artech House, 1981.
[16] M. Kobayashi, "A dispersion formula satisfying recent requirements in microstrip CAD," *IEEE Trans. Mircowave Theory Tech.*, vol. 36, pp. 1246–1250, Oct. 1988.
[17] E. Hammerstad and O. Jensen, "Accurate models for microstrip computer-aided design," in *IEEE MTT-S Int. Microwave Symp. Dig.*, Washington, DC, May 1980, pp. 407–409.

Natalia Georgieva (S'93) received the Dipl. Eng. degree in electronics from the Technical University of Varna, Varna, Bulgaria, in 1989, and the Dr. Eng. degree from the University of Electro-Communications, Tokyo, Japan, in 1997.

She is currently a Post-Doctoral Fellow at Dalhousie University Polytechnic, Halifax, N.S., Canada. Her research concerns time-domain techniques in electromagnetics and their numerical implementation to the analysis of MMIC structures and antennas.

Eikichi Yamashita (M'66–SM'79–F'84) was born in Tokyo, Japan, on February 4, 1933. He received the B.S. degree from the University of Electro-Communications, Tokyo, Japan, in 1956, and the M.S. and Ph.D. degree from the University of Illinois at Urbana-Champaign, in 1963, and 1966, respectively, all in electrical engineering.

From 1956 to 1964, he was a Research Staff Member of millimeter-wave engineering at the Electrotechnical Laboratory, Tokyo, Japan. While on leave from 1961 to 1963, and from 1964 to 1966, he studied solid-state devices in the millimeter-wave region at the Electro-Physics Laboratory, University of Illinois at Urbana-Champaign. In 1967, he became Associate Professor in the Department of Electronic Engineering, and Professor in 1977. From 1992 to 1994, he was Dean of the Graduate School, University of Electro-Communications. He served as editor of *Analysis Methods for Electromagnetic Wave Problems*, vols. 1, 2 (Norwood, MA: Artech House). Since 1956, his research work has principally been on applications of electromagnetic waves such as various microstrip transmission lines, wave propagation in gaseous plasma, pyroelectric-effect detectors in the submillimiter-wave region, tunnel-diode oscillators, wide-band laser modulators, various types of optical fibers, ultrashort electrical pulse propagation on transmission lines, and millimiter-wave imaging.

Dr. Yamashita was chairperson of the Technical Group on Microwaves, Institute of Electronics, Information and Communication Engineers (IEICE), Japan (1985–1986), and vice-chairperson of the Steering Committee, Electronics Group, IEICE (1989–1990). He was an associate editor of the IEEE Transactions on Microwave Theory and Techniques (1980–1984, 1996). He was elected chairperson of the MTT-S Tokyo Chapter (1985–1986). Since 1992, he has been a member of the MTT-S ADCOM, and since 1995, chairperson of the Chapter Operations Committee, IEEE Tokyo Section. He served as chairperson of the International Steering Committee (1990, 1994) of the Asia-Pacific Microwave Conference, which was held in Tokyo and sponsored by the IEICE.